Journal of the Mechanics and Physics of Solids 95 (2016) 755–773

Contents lists available at ScienceDirect

Journal of the Mechanics and Physics of Solids

journal homepage: www.elsevier.com/locate/jmps

Bridging micro to macroscale fracture properties in highly heterogeneous brittle solids: weak pinning versus fingering

Manish Vasoya [a,b,1], Véronique Lazarus [b,*], Laurent Ponson [a]

[a] Institut Jean Le Rond d'Alembert (UMR 7190), UPMC-CNRS, Sorbonne Universités, F-75005 Paris, France
[b] Laboratoire FAST, Univ. Paris-Sud, CNRS, Université Paris-Saclay, F-91405 Orsay, France

ARTICLE INFO

Article history:
Received 18 December 2015
Received in revised form
30 March 2016
Accepted 16 April 2016
Available online 19 April 2016

Keywords:
Brittle fracture
Homogenization
Heterogeneities
Effective toughness and fracture energy
Fingering instability
Equilibrium shape
Weak to strong crack pinning
Iterative perturbation approach

ABSTRACT

The effect of strong toughness heterogeneities on the macroscopic failure properties of brittle solids is investigated in the context of planar crack propagation. The basic mechanism at play is that the crack is locally slowed down or even trapped when encountering tougher material. The induced front deformation results in a selection of local toughness values that reflect at larger scale on the material resistance. To unravel this complexity and bridge micro to macroscale in failure of strongly heterogeneous media, we propose a homogenization procedure based on the introduction of two complementary macroscopic properties: An *apparent toughness* defined from the loading required to make the crack propagate and an *effective fracture energy* defined from the rate of energy released by unit area of crack advance. The relationship between these homogenized properties and the features of the local toughness map is computed using an iterative perturbation method. This approach is applied to a circular crack pinned by a periodic array of obstacles invariant in the radial direction, which gives rise to two distinct propagation regimes: A *weak pinning regime* where the crack maintains a stationary shape after reaching an equilibrium position and a *fingering regime* characterized by the continuous growth of localized regions of the fronts while the other parts remain trapped. Our approach successfully bridges micro to macroscopic failure properties in both cases and illustrates how small scale heterogeneities can drastically affect the overall failure response of brittle solids. On a broader perspective, we believe that our approach can be used as a powerful tool for the rational design of heterogeneous brittle solids and interfaces with tailored failure properties.

1. Introduction

Predicting the role played by small scale heterogeneities on the macroscopic fracture toughness of materials is an important challenge in mechanical engineering. Besides obvious benefits in terms of reliability, it also aims at assisting the design of multi-material components with controlled mechanical toughness combined with other controlled properties (weight, permeability, thermal or electrical conductivity, etc.). The central question is: How can we predict the fracture properties at the macroscopic scale from the knowledge of the toughness at the microscopic one? This requires the definition of effective fracture properties and a method to calculate them. An inherent difficulty of this problem is the scale and

* Corresponding author.
[1] M.V. presently is at Chemical Physics Department, Weizmann Institute of Science, Rehovot 7610001, Israel.

http://dx.doi.org/10.1016/j.jmps.2016.04.022
0022-5096/

spatial dimension separations between (i) the *bulk* elastic energy involving the structure *continuum* scale and (ii) the *surface* fracture energy associated with the local dissipation at the *microscopic* scale in the crack tip vicinity. This renders the use of classical homogenization methods based on a volume-average of bulk material inappropriate.

The role played by heterogeneities and defects on the fracture resistance are various. When crack initiation dominates the fracture process, the failure strength of a solid is not ruled by an average of its local properties, but rather by the response of a little part of it that acts as a "weak link" and is responsible for the failure of the whole solid (Weibull, 1939). When material failure involves the propagation of a crack, heterogeneities may influence the macroscopic toughness by several ways. For instance, micro-cracks may play a complex role on the crack propagation: Depending on their position and orientation, they result in enhancement or decrease of toughness (Kachanov, 1994); elastic heterogeneities have a strong influence on crack behavior and have shown potential to increase significantly fracture resistance (Gao, 1991; Dimas et al., 2014; Hossain et al., 2014); energy dissipation at the interface between elementary constituents (Barthelat and Rabiei, 2011) and crack bridging by unbroken fibers (Bower and Ortiz, 1991) are other efficient toughening mechanisms, largely present in nature (Barthelat et al., 2007; Ritchie, 2011). Crack front deformation induced by pinning of the crack on tougher zones has also a significant impact on the macroscopic toughness (Gao and Rice, 1989; Bower and Ortiz, 1991; Xia et al., 2015).

In this paper, we focus on this last effect in the context of brittle fracture, and make the assumption of planar propagation that amounts to exclude the crossing of obstacles through out-of-plane crack excursions. This situation prevails for cracks propagating within a textured interface, as encountered in multifunction double glazing or in electronic chips. It is also representative of crack pinning phenomena at play in many materials at the scale of their microstructure and represents an important step toward the description of the more complex situation of a brittle crack propagating through a three-dimensional heterogeneous medium. The basic mechanism is that the crack front advance is slowed down in tougher regions, so that the geometry of the crack line evolves during propagation. These deformations themselves change the local loading along the front that controls the zones of the toughness map visited by the front, hence the macroscopic toughness. This coupled problem involving geometry and loading changes, belongs to the realm of free-discontinuity problems. Another difficulty inherent to that situation is that it cannot be understood within the frame of 2D fracture mechanics, contrary to most of the previously mentioned toughening mechanisms, since it necessarily implies the description of the failure process through the evolution of the crack front and not one crack tip alone.

Perturbation approach proposed by Rice (1989), based on Bueckner (1987)'s weight functions, is an efficient way to address such problems. This approach provides the first-order expression of the variation of the stress intensity factor (SIF) induced by some small, but otherwise arbitrary coplanar perturbation of the front. The expression corresponding to the half-plane crack geometry established by Rice (1985) has been extensively used, thanks to its relative simplicity. A length scale is however lacking for this simple geometry restricting its usefulness to qualitative purposes. To fill this gap, the approach has been extended to finite size cracks, especially circular (Gao and Rice, 1987; Gao, 1988) and tunnel-cracks (Leblond et al., 1996; Lazarus and Leblond, 2002; Pindra et al., 2010) (see also Lazarus, 2011 for a review). More recently, it has been extended to the case of a half-plane crack lying on the mid-plane of a semi-infinite plate (Legrand et al., 2011), leading to quantitative agreement (Patinet et al., 2011, 2013a) with Dalmas et al. (2009)'s clivage experiments in which a crack is pinned by a stripe of tougher material.

For weakly heterogeneous materials, those expressions have been used to obtain first-order estimations of the effective fracture toughness. Gao and Rice (1989) considered periodic arrays of weak obstacles and studied their effect on the remote loading: After a transient phase where the load has to be increased to allow the penetration of the crack in between the obstacles, the propagation becomes unstable in the sense that it occurs at a lower loading. They estimated the critical load corresponding to the onset of instability for several geometries of obstacles. Roux et al. (2003) followed by Patinet et al. (2013b) and Demery et al. (2014) considered the case of disordered arrangements of toughness heterogeneities. They showed that (i) in the absence of dynamical phases during the propagation (weak pinning regime), the effective toughness is equal to its spatial average value while (ii) in the presence of micro-instabilities (strong pinning regime) following collective depinning of the front from impurities, the effective toughness is increased. Here we aim to study how in the first case, that is in the absence of any micro-instability, large front deformations can actually affect the macroscopic resistance to failure. In particular, we aim to answer to the following question: How does the effective toughness depart from the mean one for increasing strength of heterogeneities?

Whether of the first or second order (Leblond et al., 2012; Vasoya et al., 2013; Willis, 2013; Vasoya et al., 2016), asymptotic studies remain essentially restricted to small front perturbations. For larger perturbations arising from higher toughness contrasts, the use of numerical methods becomes mandatory. The finite perturbation method, proposed by Rice (1989) and developed numerically by Bower and Ortiz (1990), Lazarus (2003) and Favier et al. (2006) is based on multiple numerical iterations of the previously introduced first-order formula. Some examples presented in Bower and Ortiz (1990), (1991), Lai et al. (2002) and Lazarus (2003), have shown its ability to track the crack front when strolling through some heterogeneous media, hence to deal with our problem.

Here this method is used to address the problem of a circular crack pinned by a periodic array of obstacles with radial symmetry, *i.e.* invariant along the propagation direction. The *apparent toughness* defined from the loading required to make the crack propagate and the *effective fracture energy* defined from the rate of energy released by unit area of crack advance are computed as a function of the obstacles strength and width. Surprisingly, the macroscopic fracture properties do not vary continuously with the microscopic ones. Instead, our calculation brings out two separate branches: For weak and small obstacles, effective properties remain close to the material average toughness while strong obstacles of large size result in a

dramatic drop of the resistance that is then essentially governed by the toughness of the weakest material.

To unravel these observations, we investigate the crack behavior at the local scale and study the geometry of the front as it penetrates into the obstacles. We evidence two distinct propagation regimes that correspond to the two regimes evidenced at the global scale on the effective fracture properties. At small obstacle strength and width, in the so-called *weak pinning regime*, the whole crack front advances by maintaining a stationary shape. At larger strength and width, we observe a *fingering regime* characterized by the continuous growth of localized regions of the fronts in between obstacles while the rest of the front remains trapped. The way the global effective properties emerge from these specific local growth mechanisms is discussed in both regimes.

The paper is organized as follows. In Section 2, we introduce the homogenization procedure from which the effective fracture properties are defined, namely the apparent toughness and the effective fracture energy. The iterative perturbation approach used to compute these quantities from the features of the local toughness map is described in Section 3. This approach is first applied in Section 4 in the limit of weak obstacles, and compared with first-order analytical predictions for validation. Variations of the effective failure properties for larger toughness contrasts are presented in Section 5 as a function of the obstacle strength and width. In Section 6, the weak pinning and fingering crack propagation regimes are described at the local scale. In Section 7, the observations made at the local scale are used to explain the behavior of the macroscopic fracture properties. Finally, the conclusions and implications of the present study, and directions for future work are presented in Section 8.

2. Homogenization procedure

2.1. Heterogeneous problem at the microscale

Consider a solid body containing a circular planar crack $\mathcal{F}$ and made of a linear elastic material with homogeneous elastic constants E and ν, but heterogeneous fracture toughness $\kappa_c(M)$ or, equivalently, fracture energy $\gamma_c(M)$. The crack is supposed to be sufficiently far from the body's boundary so that one can safely assume that (i) the body is infinite and (ii) the tensile loading σ is applied at infinity (Fig. 1). We assume pure mode I tensile loading and denote $\kappa(M)$ the mode I Stress Intensity Factor (FIC) and $\gamma(M)$ the energy release rate, both defined locally at point M. The crack advance satisfies locally, at each instant, Irwin's criterion

$$\begin{cases} \kappa(M) < \kappa_c(M) \;\Rightarrow\; \text{no crack advance} \\ \kappa(M) = \kappa_c(M) \;\Rightarrow\; \text{crack propagation} \end{cases} \tag{1}$$

or Griffith's one

$$\begin{cases} \gamma(M) < \gamma_c(M) \;\Rightarrow\; \text{no crack advance} \\ \gamma(M) = \gamma_c(M) \;\Rightarrow\; \text{crack propagation.} \end{cases} \tag{2}$$

In the following, the external loading σ is adjusted so that the local driving $\kappa(M)$ (resp. $\gamma(M)$) never exceeds the material toughness $\kappa_c(M)$ (resp. $\gamma_c(M)$). This ensures that the propagation remains quasistatic and discards any dynamical dissipation.

Criteria of Eqs. (2) and (1) are equivalent, γ and γ_c being linked to κ and κ_c by Irwin (1957)'s relation:

$$\gamma = \frac{1-\nu^2}{E}\kappa^2 \quad \text{and} \quad \gamma_c = \frac{1-\nu^2}{E}\kappa_c^2 \tag{3}$$

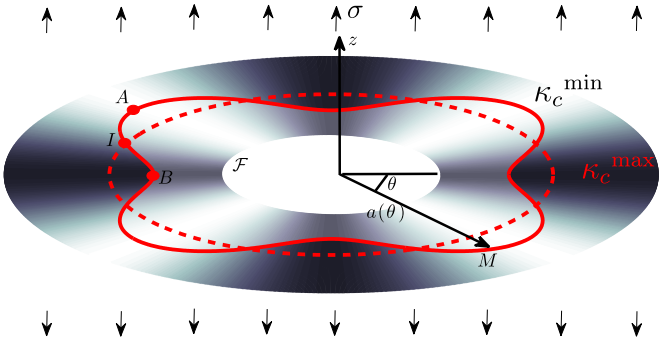

Fig. 1. Circular crack submitted to a remote tensile loading growing in a plane that contains $k=4$ obstacles of strength $\Delta = \frac{\kappa_c^{\max} - \kappa_c^{\min}}{\kappa_c^{\max} + \kappa_c^{\min}}$ aligned in the propagation direction.

2.2. Homogeneous problem at the macroscale

Homogenization consists in replacing the problem at the microscale by an equivalent homogeneous problem at the macroscale. For this, we propose

(i) To replace the deformed crack front by a circular one of the same area, that is

$$a = \sqrt{\frac{S}{\pi}} \tag{4}$$

where S is the area of the deformed crack and a the radius of the equivalent circular crack.

(ii) To replace Irwin's local criterion by a global one $K \le K_c^a$, where the macroscopic SIF, denoted K, is defined by the one of the equivalent circular crack

$$K \equiv \frac{2}{\sqrt{\pi}}\sigma\sqrt{a}. \tag{5}$$

(iii) To replace Griffith's local criterion by $G \le G_c^a$, the macroscopic energy release rate G being given by

$$G = \frac{\int_{\mathcal{F}} \gamma(M)\delta(M)\,\mathrm{d}s(M)}{\int_{\mathcal{F}} \delta(M)\,\mathrm{d}s(M)}, \tag{6}$$

where $\delta(M)$ is the normal distance between $\mathcal{F}$ and an infinitesimally close subsequent position of the crack front.

The introduction of *two* a priori independent homogenized quantities K_c^a and G_c^a calls for a few comments. The *instantaneous toughness* K_c^a is defined from the loading required to make propagate an equivalent circular crack, as proposed by Gao and Rice (1989). This approach prevails in most experimental situations where a loading is imposed to a fractured sample and the average crack length is measured *e.g.* through optical means. A large toughness reveals an enhanced resistance in terms of critical loading at failure that is of direct relevance for material and structure design. We also introduce the *instantaneous fracture energy* G_c^a defined from the evolution of the macroscopic energy release rate G with the crack size, as proposed by Hossain et al. (2014) in the context of 2D heterogeneous media. This derives from the application at the global scale of Griffith's energy conservation law that describes the transfer of mechanical energy into fracture energy, ensuring $G = G_c^a$ during failure.

By construction, both K_c^a and G_c^a depend on the crack size a and correspond to the instantaneous values of the propagation thresholds. For the microstructure studied hereafter, invariant along the propagation direction, they both reach a stationary value after an initial transient regime. We use this limit to define the macroscopic failure properties

$$K_c = \lim_{a\to\infty} K_c^a \quad \text{and} \quad G_c = \lim_{a\to\infty} G_c^a \tag{7}$$

that we call *apparent toughness* and *effective fracture energy*, respectively.

For a *homogeneous* distribution of fracture properties, the crack remains circular and the problem at the global scale is equivalent to the one at the local scale, hence $K = \kappa$ and $G = \gamma$, that remains true at the propagation threshold. Therefore, Irwin's relation $\gamma_c = \frac{1-\nu^2}{E}\kappa_c^2$ between local material properties remains valid for the homogenized quantities $G_c = \frac{1-\nu^2}{E}K_c^2$ too. The survival of this equivalence between a loading and an energy based criterion at the global scale for *heterogeneous* media is one of the central points of this study. We return to this issue in Section 7.

2.3. From the micro to the macroscale

The macroscopic SIF K and elastic energy release rate G are equal to K_c^a and G_c^a only if a grows. At the microscale, it means that at least some part of the crack front advances that is $\kappa = \kappa_c$ is reached at least at one point, which is equivalent to

$$\max_{M\in\mathcal{F}} \frac{\kappa(M)}{\kappa_c(M)} = 1. \tag{8}$$

In practice, the steps required to link the micro to the macroscale are as follows:

(i) The quasistatic propagation problem is solved at the microscale following the propagation law of Section 2.1. More precisely, for each subsequent crack position, the onset loading σ_c is determined from Eq. (8) as well as the corresponding front shape and the local values of $\kappa(M)$ and $\gamma(M)$.

(ii) K and G are computed using their definitions (5) and (6), respectively.

(iii) the instantaneous failure properties K_c^a and G_c^a are obtained by identification with K and G.

(iv) K_c and G_c are then determined from the asymptotic values of K_c^a and G_c^a in the long crack growth limit.

3. Numerical procedure

The homogenization method proposed above is quite general and may be easily transposed to other geometries, as e.g. cracks with a straight front on average. The only practical hurdle may be the numerical resolution of the quasistatic propagation problem at the microscale. For the planar crack problem considered here, perturbation approaches (Rice, 1989; Bower and Ortiz, 1990; Lazarus, 2011) are an efficient way to solve it. In practice, we extended the numerical code of Lazarus (2003) in the following way. We start from an initial circular crack of radius a_0 for which

$$\kappa(M) = \frac{2}{\sqrt{\pi}}\sigma\sqrt{a_0}. \tag{9}$$

We introduce the following dimensionless SIF $\hat{\kappa}$ defined by

$$\kappa(M) = \frac{2}{\sqrt{\pi}}\sigma\sqrt{a_0}\ \hat{\kappa}(M). \tag{10}$$

$\hat{\kappa}$ depends on the crack shape and size, but is independent of the applied loading due to linearity of the elasticity problem. The crack evolution is then solved iteratively by successive small normal perturbations δa of the front. We detail below how to update the crack shape and the local SIF κ, on the one hand, and the macroscopic quantities σ_c, K_c^a, G_c^a, on the other hand.

3.1. Determination of the crack advance δa

Irwin's propagation law of Eq. (1) is regularized by Paris'law (Lazarus, 2003)

$$\delta a(M) = \delta a_{\max}\left(\frac{\kappa(M)}{\kappa_c(M)}\right)^{\beta} \tag{11}$$

using a large exponent $\beta \gg 1$.

This procedure is analogous to the viscoplastic regularization in plasticity. It retrieves Irwin's threshold behavior (1), since:

$$\begin{cases} \delta a(M) \sim 0 & \text{if } \kappa(M) < \kappa_c(M) \\ \delta a(M) \sim \delta a_{\max} & \text{if } \kappa(M) = \kappa_c(M) \end{cases} \tag{12}$$

and hence, ensures quasistatic crack propagation.

Advantage of using Paris' law is that the crack advance at all steps is provided explicitly. Disadvantage is that some numerical instability may occur for some values of the spatial (number of nodes N) and temporal discretization (given by $\delta a_{\max}$), as when Eulerian explicit scheme is used to solve classical partial differential equations. This point has been studied in detail in Vasoya (2014) and a map of the numerical stability is provided in Fig. A1 of Appendix A.

3.2. Update of the stress intensity factor $\hat{\kappa}$

The dimensionless SIF $\hat{\kappa}$ is updated by using Rice (1989)'s first-order perturbation formula

$$\delta\hat{\kappa}(M_0) = \frac{1}{2\pi} PV \int_{\mathcal{F}} \frac{w(M, M_0)}{d^2(M, M_0)}\hat{\kappa}(M)[\delta a(M) - \delta_* a(M)]\, \mathrm{d}s(M). \tag{13}$$

In this equation, s denotes the curvilinear abscissa, $d(M, M_0)$ is the distance between two points, $\delta_* a(M)$ corresponds to a translation of the crack front and is introduced to ensure the existence of the Principal Value (PV) integral. Its contribution to $\delta\hat{\kappa}(M_0)$ is zero here, since it leaves the elasticity problem unchanged thanks to the hypothesis of infinite solid. The non-local behavior of the SIF with respect to the front geometry emerges from the long-range interactions between different zones of the front that are mediated through the bulk elasticity. This confers a long-range elasticity to the crack front which is described by the dimensionless kernel $w(M, M_0)$ updated using a similar formula

$$\delta w(M_1, M_0) = \frac{d^2(M_1, M_0)}{2\pi} PV \int_{\mathcal{F}} \frac{w(M_1, M)}{d^2(M_1, M)}\frac{w(M_0, M)}{d^2(M_0, M)}[\delta a(M) - \delta_{**} a(M)]\, \mathrm{d}s(M). \tag{14}$$

Here, $\delta_{**} a(M)$ corresponds to the composition of translation, rotation and homothety which ensures the existence of PV while leaving the kernel unchanged, again since the solid is supposed here to be infinite.

3.3. Determination of the macroscopic properties

The critical loading is then obtained by introducing (10) in (8)

$$\sigma_c = \frac{\sqrt{\pi}}{2\sqrt{a_0}}\left[\max_{M\in\mathcal{F}} \frac{\hat{\kappa}(M)}{\kappa_c(M)}\right]^{-1}, \tag{15}$$

and from it, the macroscopic fracture properties K_c^a and G_c^a following the methods described in Section 2.2. More precisely, K_c^a is given by Eq. (5) with $\sigma = \sigma_c$, the equivalent radius a being itself obtained by updating the crack area S using the first-order formula $\delta S = \int_{\mathcal{F}} \delta a(M)\, \mathrm{d}s(M)$. The effective fracture energy G_c^a is obtained from Eq. (6) and reads

$$G_c^a = \frac{4}{\pi}\left(\frac{1-\nu^2}{E}\right)\sigma_c^2 a_0 \ \frac{\int_{\mathcal{F}} \hat{\kappa}^2(M)\delta a(M)\, \mathrm{d}M}{\int_{\mathcal{F}} \delta a(M)\, \mathrm{d}M}. \tag{16}$$

Besides the knowledge of $\hat{\kappa}$, another dimensionless useful SIF $\tilde{\kappa}$ defined by

$$\tilde{\kappa} = \sqrt{\frac{a_0}{a}}\hat{\kappa} \tag{17}$$

is computed. Both $\hat{\kappa}$ and $\tilde{\kappa}$ depend only on the geometry of the crack front (and not on the loading). Whereas $\hat{\kappa}$ depends on the crack shape and size, $\tilde{\kappa}$ is only shape dependent. The total SIF κ is derived from the definitions (10) and (15). $\hat{\kappa}$, $\tilde{\kappa}$ and κ are used in the sequel depending on the needs.

4. Application to a circular crack pinned by a periodic array of obstacles

In the following, we consider the case of a circular crack propagating in the toughness field

$$\kappa_c(M) = \kappa_c(\theta) = \overline{\kappa_c}[1 + \Delta\cos(k\theta)] \tag{18}$$

of mean value $\overline{\kappa_c}$ that contains k obstacles, as schematized in Fig. 1 for $k=4$. This local toughness is invariant in the radial direction depicting obstacles infinitely elongated along the crack propagation, but varies sinusoidally along the crack front direction. As a result, the fracture plane displays a k-fold rotational symmetry characterized by two parameters:

(i) the dimensionless obstacle strength or toughness contrast $\Delta = \frac{\kappa_c^{\max} - \kappa_c^{\min}}{\kappa_c^{\max} + \kappa_c^{\min}}$. To ensure positive toughness everywhere in the fracture plane, the contrast is comprised in between $0 \le \Delta \le 1$;
(ii) the number k of obstacles or equivalently, the dimensionless obstacle width $1/k$ that gives the fraction of the crack front covered by one obstacle, its actual width being given by $\xi = 2\pi a/k$. To ensure continuity of the toughness field in $\theta = 0$, one considers only integer values of $k \ge 1$.

Using Irwin's relation (3), one gets the fracture energy field

$$\gamma_c(\theta) = \frac{\overline{\gamma_c}}{1 + \frac{\Delta^2}{2}}[1 + 2\Delta\cos(k\theta) + \Delta^2\cos^2(k\theta)] \tag{19}$$

where the mean fracture energy is given by

$$\overline{\gamma_c} \equiv \frac{1}{2\pi}\int_0^{2\pi} \gamma_c(\theta)\, \mathrm{d}\theta = \frac{1-\nu^2}{E}\overline{\kappa_c}^2\left(1 + \frac{\Delta^2}{2}\right). \tag{20}$$

For this problem, if $\Delta = 0$, that is the material is homogeneous ($\kappa_c^{\min}/\kappa_c^{\max} = 1$), the crack remains circular since it is stable toward any geometrical perturbation (Gao and Rice, 1987). If $\Delta \neq 0$, that is $\kappa_c(M)$ is heterogeneous, the crack advance is affected by the local toughness field and the circular shape deforms. The limiting case $\Delta = 1$ corresponds to infinitely strong obstacles or, equivalently, to infinitely weak regions between obstacles ($\kappa_c^{\min}/\kappa_c^{\max} = 0$).

4.1. Analytical first-order resolution for small toughness contrast

Suppose now that the heterogeneity contrast is small, that is $\Delta \ll 1$. Using Gao and Rice (1987)'s expression for $\kappa(\theta)$ valid for slightly perturbed circular cracks, one shows that, in polar coordinates, $a(\theta) = a + \Delta a/2\cos(k\theta)$ with

$$\frac{\Delta a}{a} = -\frac{4\Delta}{k-1} \tag{21}$$

satisfies the equilibrium condition $\kappa(M) = \kappa_c(M)$ along the whole front for σ_c given by $\frac{2}{\sqrt{\pi}}\sigma_c\sqrt{a} = \overline{\kappa_c}$. Fig. 2 compares the numerical results for $k=4$ and $\Delta = 0.2$ with the first-order analytical solution: an agreement within 1% is found.

From the front geometry and the definitions (5) and (6), one calculates the homogenized properties

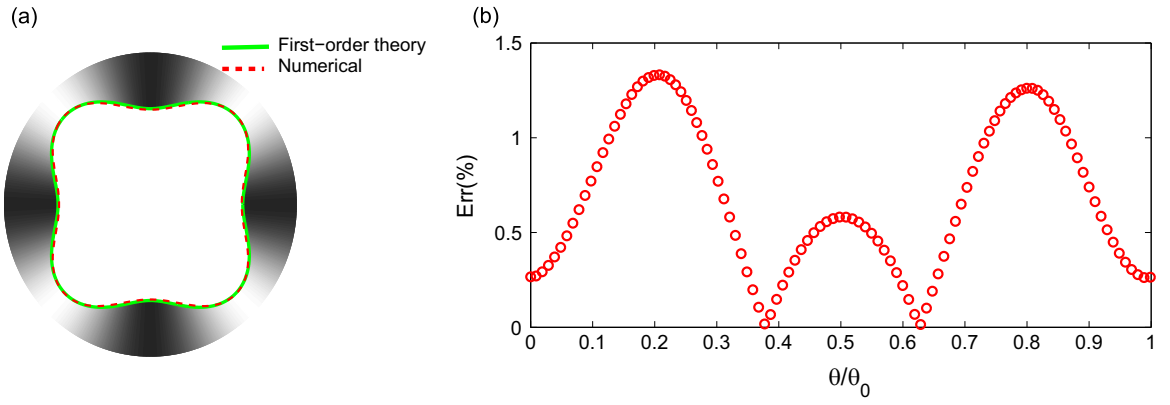

Fig. 2. Comparison of the numerical results with the first-order asymptotic expression of the front shape $a(\theta)$ for $k=4$ and $\Delta = 0.2$: (a) Front geometry in the stationary regime; (b) relative error between the numerical and first-order theoretical values of $a(\theta)$.

$$K_c^a/\overline{\kappa_c} = G_c^a/\overline{\gamma_c} = 1 \quad \forall\, k > 1. \tag{22}$$

valid at the linear order in Δ (see Appendix D). It shall be noticed that an equilibrium position satisfying $\kappa(M) = \kappa_c(M)$ along the front cannot be found in the particular case $k=1$ as clear from Eq. (21). Indeed, this particular toughness field would produce front perturbations that correspond to a translation of the initial circular crack. And this perturbation mode is neutrally stable under the uniform loading conditions considered here as noticed by Gao and Rice (1987), which means that the SIF stays uniform hence cannot match with an heterogeneous toughness field.

4.2. Higher order numerical resolution for arbitrary large contrast

Numerical simulations with different wavenumbers k and toughness contrasts Δ are performed. In the following, the Paris' law exponent $\beta = 25$ is chosen which has been verified to give converging results. The spatial discretization step along the front is chosen to be substantially smaller than the obstacle width. In practice, the number of nodes is increased as the front deforms up to a maximum value of 60 nodes per period. The temporal discretization is chosen to ensure the stability of the numerical scheme (see Appendix A).

In the following, we assume that the front shape remains periodic during propagation, in agreement with the periodicity of the toughness map. This assumption is used to decrease the computational cost of the simulations: Even though the kernel w is not fully periodic,[2] it allows to limit the calculation of $\hat{\kappa}$ and δa to one period.

5. Homogenized fracture properties

5.1. Apparent toughness

The evolution of the critical loading σ_c and of K_c^a is explored in Fig. 3. We first discuss their values for $a = a_0$. Prior to initiation, the crack is circular so the value of κ is uniform along the front and equal to the macroscopic SIF K. As a result, the dimensionless SIF introduced in Eq. (10) is $\hat{\kappa} = \sqrt{a/a_0} = 1$. Using Eq. (8), the critical loading at initiation $a = a_0$ verifies

$$\frac{2}{\sqrt{\pi}}\frac{\sigma_c\sqrt{a_0}}{\overline{\kappa_c}} = 1 - \Delta.$$

from which follows the toughness at initiation $K_c^a/\overline{\kappa_c} = 1 - \Delta$. Here, the crack starts to grow when at least one point of the front fulfills $\kappa = \kappa_c$. This is satisfied first in $\theta_A = \frac{(1+2n)\pi}{k}$ for $0 \le n \le k-1$, i.e. for points A located between obstacles in the weakest part of the interface (see Fig. 1).

During the propagation phase, two regimes can be distinguished:

(i) An initial transient regime during which K_c^a increases. The loading is here essentially fixed by the value of the SIF in A where the condition $\kappa = \kappa_c$ is first reached, that is $\frac{2}{\sqrt{\pi}}\sigma_c\sqrt{a}\,\tilde{\kappa}(A) = \kappa_c^{\min}$. Since $\tilde{\kappa}(A)$ decreases as the crack advances and deforms (Gao and Rice, 1987), the loading σ_c and therefore K_c^a increase.

(ii) A stationary regime reached soon after peak load where σ_c varies inversely proportionally to $1/\sqrt{a}$ and so K_c^a remains asymptotically constant. This limit corresponds to the apparent toughness K_c.

[2] It is somehow periodic since $w(s+T, s'+T) = w(s, s')$, but not fully since $w(s+T, s') \neq w(s, s')$.

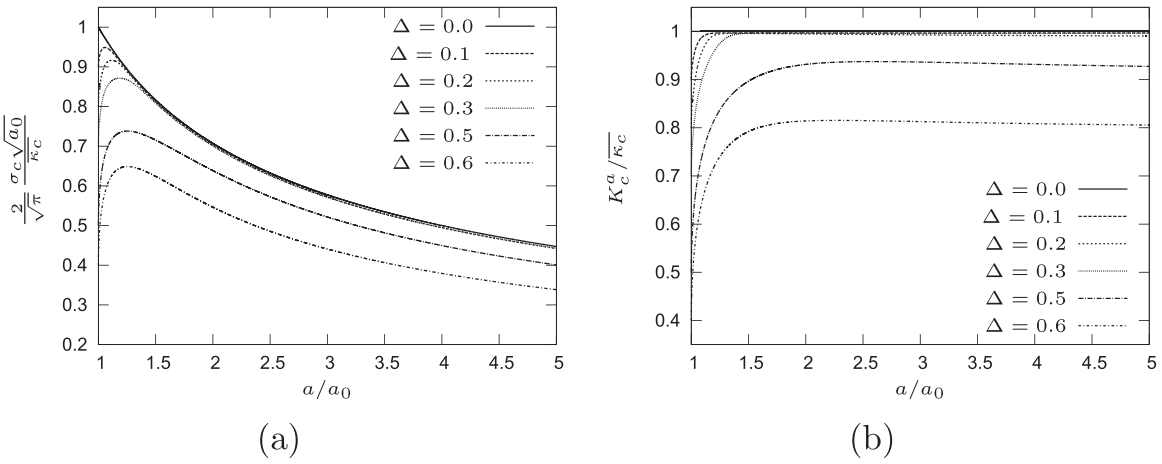

Fig. 3. Evolution of (a) the critical loading σ_c and (b) the instantaneous toughness K_c^a during crack propagation for k=4 obstacles.

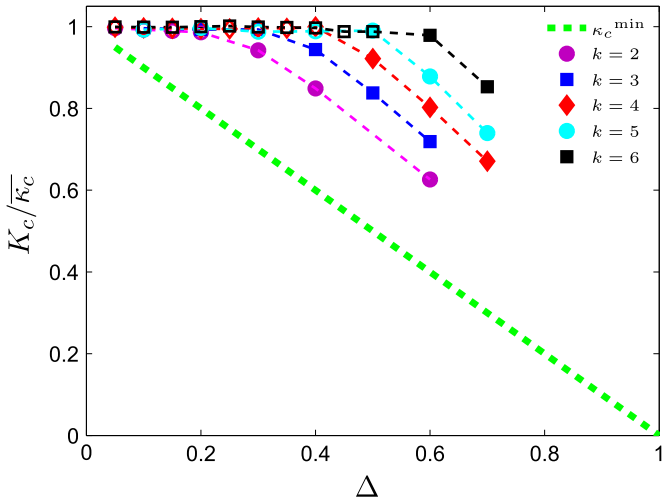

Fig. 4. Effect of the microscale fracture properties, the obstacle strength Δ and their number k, on the apparent toughness. The straight dotted green line corresponds to the minimum value $\kappa_c^{\min}/\overline{\kappa_c} = 1 - \Delta$ of the toughness field. (For interpretation of the references to color in this figure caption, the reader is referred to the web version of this paper.)

This behavior reminds the so-called *R*-curves characteristic of quasi-brittle and ductile failure that are reminiscent of the transient increase of the damage activity at the crack tip close to initiation. Remarkably, the transient increase of the SIF takes place here in a perfectly brittle material. This behavior is actually general and results from the heterogeneous nature of the toughness field: The crack explores first the *weakest* region of the fracture plane where the Griffith's condition is first reached. The front deformation thus generated, redistributes the local driving force along the crack line allowing the progression in tougher and tougher regions, but at the price of a larger applied loading, and so an increase of the instantaneous toughness K_c^a. A stationary regime may eventually be reached when Irwin's criterion (1) is satisfied everywhere along the front.

The apparent material toughness K_c is now represented as a function of the microscopic parameters on Fig. 4. Two regimes are evidenced:

(i) For weak obstacles, $\Delta < \Delta_c(k)$, the apparent toughness cannot be distinguished from the average value $\overline{\kappa_c}$ of the toughness field.
(ii) For strong obstacles, $\Delta > \Delta_c(k)$, the apparent toughness clearly deviates from $\overline{\kappa_c}$. It decays similarly to $\kappa_c^{\min}$, indicating that the crack growth is essentially governed by the *weakest* regions of the fracture plane.

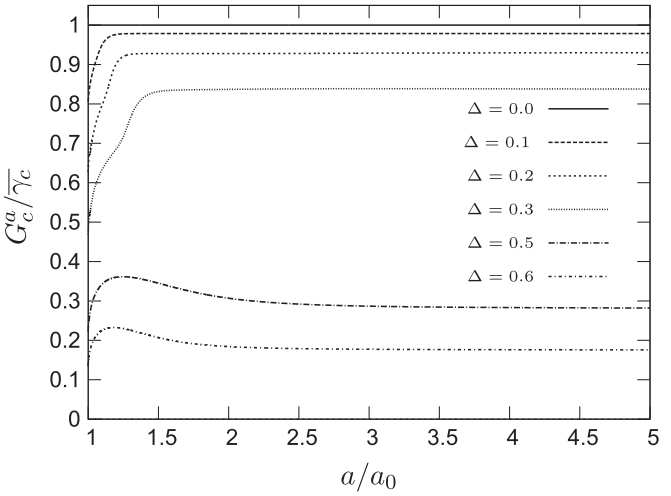

Fig. 5. Evolution of the instantaneous fracture energy G_c^a for $k=4$ obstacles.

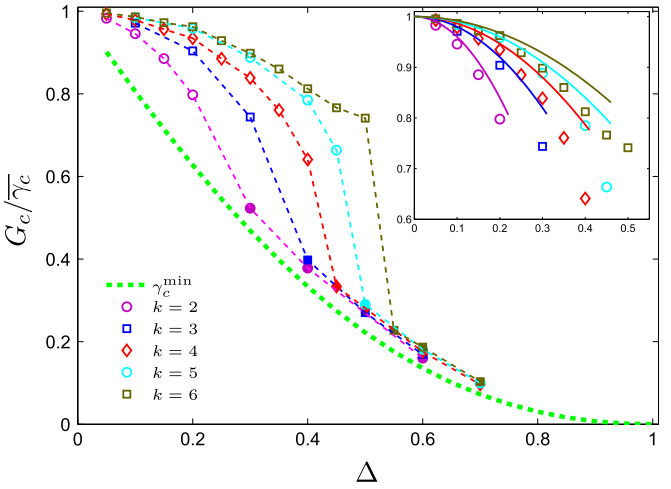

Fig. 6. Effect of the obstacle strength Δ and their number k on the effective fracture energy. The green dotted line corresponds to the minimum value $\gamma_c^{\min}/\overline{\gamma_c} = (1-\Delta)^2/(1+\Delta^2/2)$ of the fracture energy field, the other dotted lines are guides to the eyes. The inset is a zoom of the curves showing the agreement, in the limit $\Delta \ll 1$, between the second order prediction (solid lines) of Eq. (24), and the numerical values. (For interpretation of the references to color in this figure caption, the reader is referred to the web version of this paper.)

5.2. *Effective fracture energy*

We now turn to the study of the effective fracture energy. The evolution of its instantaneous value G_c^a is shown in Fig. 5 for $k=4$ and display a behavior qualitatively similar to the toughness K_c^a: Its initial value is set by the minimum $\gamma_c^{\min}/\overline{\gamma_c} = \frac{(1-\Delta)^2}{1+\frac{\Delta^2}{2}}$ of the fracture energy field given in Eq. (19). Its further evolution shows a R-curve like behavior characterized by an initial transient regime followed by a plateau that defines the effective fracture energy G_c. However, this initial transient regime does not show a monotonical increase for *all* obstacle strengths: For $\Delta < \Delta_c(k)$, G_c^a increases monotonically while for $\Delta > \Delta_c(k)$, it increases and then decreases before reaching a stationary value.

This difference also reflects on the value of the effective fracture energy G_c shown in Fig. 6 as a function of the local failure parameters: For weak obstacles $\Delta < \Delta_c(k)$, the effective toughness slightly decays with Δ, but remains close to the average value $\overline{\gamma_c}$ of the fracture energy field. While above some critical contrast value $\Delta_c(k)$, the effective fracture energy suddenly drops to follow another branch corresponding to the minimal value $\gamma_c^{\min}$ of the fracture energy field.

The discontinuous evolution of the effective fracture energy with the obstacle strength Δ illustrates a characteristic feature of crack propagation problems in heterogeneous media: Since the effective fracture properties reflect the long-time state reached by the crack after its evolution through the heterogeneous fracture plane, a small variation in the material features at the local scale may result in a large variation in the effective resistance at the large scale. The observation of a

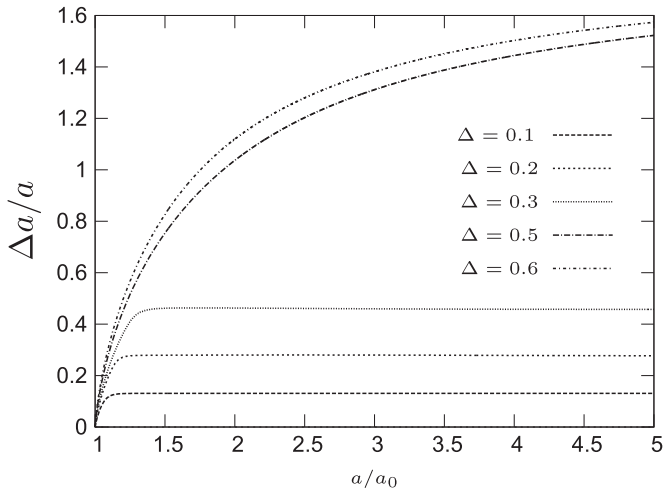

Fig. 7. Evolution of the relative front deformation during crack propagation for $k=4$ obstacles.

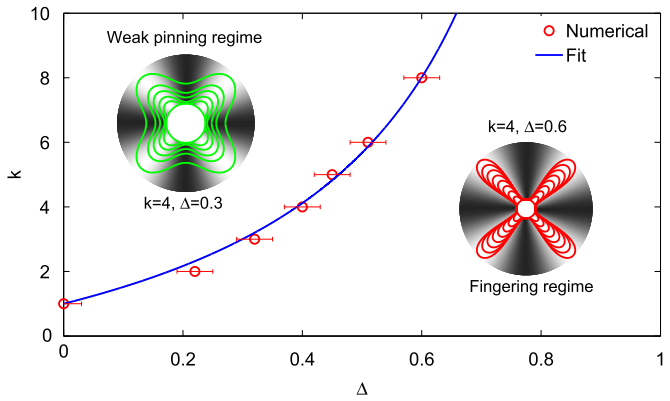

Fig. 8. Propagation regimes of a circular crack through an array of k obstacles of strength Δ. In this diagram, the upper region of the (k, Δ) space corresponds to a *weak pinning* regime where the crack reaches a stationary shape after an initial transient, while the lower region corresponds to a *fingering* regime characterized by infinitely growing petals.

transition between a fracture energy G_c close to the average value $\overline{\gamma_c}$, to a branch close to the weakest value $\gamma_c^{\min}$, indicates a drastic change of the crack propagation mode that is now investigated.

6. Crack propagation regimes: From weak pinning to fingering

6.1. Evolution of the crack front deformation

The observation of two distinct failure behaviors at the macroscale brings us to the study of the crack growth mechanisms at the microscale. Figure 7 shows the evolution for $k = 4$ of the front deformation amplitude $\frac{\Delta a}{a} \equiv \frac{a(A)-a(B)}{a}$ (see Fig. 1 for definition of A and B). For weak obstacles $\Delta < \Delta_c \simeq 0.4$, the relative front deformation rapidly saturates underlining that the crack reaches a stationary configuration. On the contrary, the front deformation for strong obstacles $\Delta > \Delta_c$ shows a steady increase, revealing that the crack configuration constantly evolves during crack growth.

6.2. Identification of the propagation regimes in the parameter space of the toughness field

The systematic study of the evolution of the crack front deformation as a function of the number k of obstacles and their strength Δ allows us to define two separated regions in the (k, Δ) parameters space of Fig. 8, that associate with two distinct growth regimes:

- A weak pinning regime taking place for small obstacle strengths $\Delta < \Delta_c(k)$ where, after an initial transient, the front

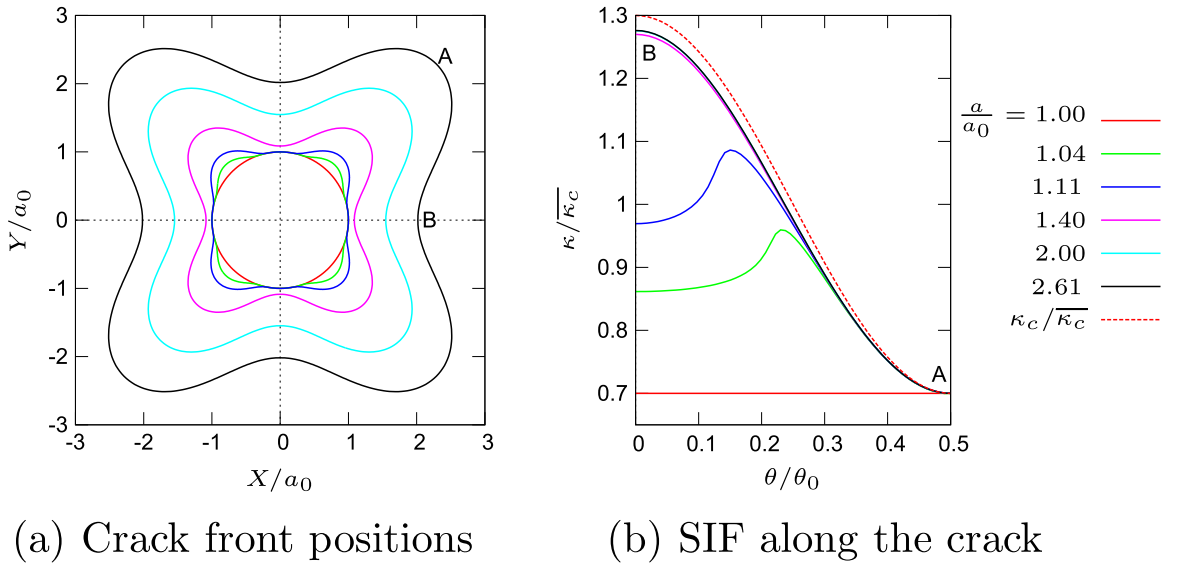

Fig. 9. Successive crack front positions and SIF along the crack front during propagation in the weak pinning regime for $\Delta = 0.3$ and $k=4$. (For interpretation of the references to color in this figure caption, the reader is referred to the web version of this paper.)

reaches a stationary shape characterized by a finite petal size.

- A fingering strong pinning regime taking place for large obstacle strengths $\Delta > \Delta_c(k)$ where localized regions of the front remain trapped by the obstacles while the other ones propagate in-between forming elongated fingers. In that regime, the crack shape never becomes stationary and looks like a flower with infinitely growing petals. Despite different underlying mechanisms, this morphology is not without reminding the digital instability emerging in soft elastic films when used as joints between relatively rigid bodies (Ghatak et al., 2000; Saintyves et al., 2013) or the fingers destabilizing the interface between two immiscible fluids of different viscosity (Saffman and Taylor, 1958).

From Fig. 8, we see that, as the number k of obstacles increases, the range of toughness contrast Δ for which crack propagation reaches a stationary state increases. The border between both regimes is well described by $\Delta_c = (k-1)/(k+3.65)$ represented by the dotted line in Fig. 8. This allows us to extrapolate the critical contrast $\lim_{k\to\infty}\Delta_c(k) = 1$ in the limit of an infinite number of obstacles. Since $k = \frac{2\pi a}{\xi}$, this implies that the fingering domain shrinks to zero when the heterogeneity size ξ becomes negligible in comparison with the crack radius a. On the contrary, in the other limit $k=1$, Δ_c shrinks to 0, which means that a weak pinning regime can never be reached as already noticed in Section 4.1.

6.3. Local propagation mechanisms

We now explore the typical features of the crack growth in each of these regimes by focusing on the particular case $k=4$ for which the critical transition strength $\Delta_c \simeq 0.4$ (see Fig. 8). We choose $\Delta = 0.3$ for the weak pinning regime and $\Delta = 0.6$ for the fingering one. Other values of k give similar results that are given for sake of completeness in Appendix B in the range $k = 1-6$.

The successive positions of the crack front and the corresponding local values of the SIF $\kappa(\theta)$ along one-half of a petal are shown in Fig. 9 for the weak pinning regime. Those are compared with the local toughness κ_c given by the dashed line. At initiation, the crack represented in red is initially circular, and the SIF is uniformly distributed. The propagation threshold is reached around A, so that only the region of the crack line close to A advance whereas the other part of the front is pinned. As a result, the front deforms and the SIF increases around B (green and blue front positions) until reaching a configuration around $a \sim 1.4a_0$ for which $\kappa(\theta) \sim \kappa_c(\theta)$ everywhere (purple, cyan and black positions). The local equilibrium conditions are then preserved all along the front as the crack continues to grow and maintain then the same stationary shape.

The fingering propagation regime is investigated through similar plots in Fig. 10. Like the other regime, the SIF is uniformly distributed at initiation (red front position), and then increases around point B (green and blue positions). However, its value starts to decrease around $a \sim 1.6a_0$ before the largest toughness value $\kappa_c(B)$ has been reached (purple, turquoise and gray positions). As a consequence, the point B never reaches the propagation threshold and remains trapped while region A advances by forming increasingly long fingers. Contrary to the previous regime, the front configuration is constantly changing, even though the shape of the finger tips actually remains stationary.

To summarize, the existence of a weak pinning regime relates to the increase of the SIF at point B located in the toughest region of the fracture plane until the propagation threshold $\kappa(B) = \kappa_c^{\max}$ is reached. After that transient, the equilibrium condition $\kappa = \kappa_c$ is satisfied all along the front. The corresponding equilibrium crack shape is then kept unchanged during its

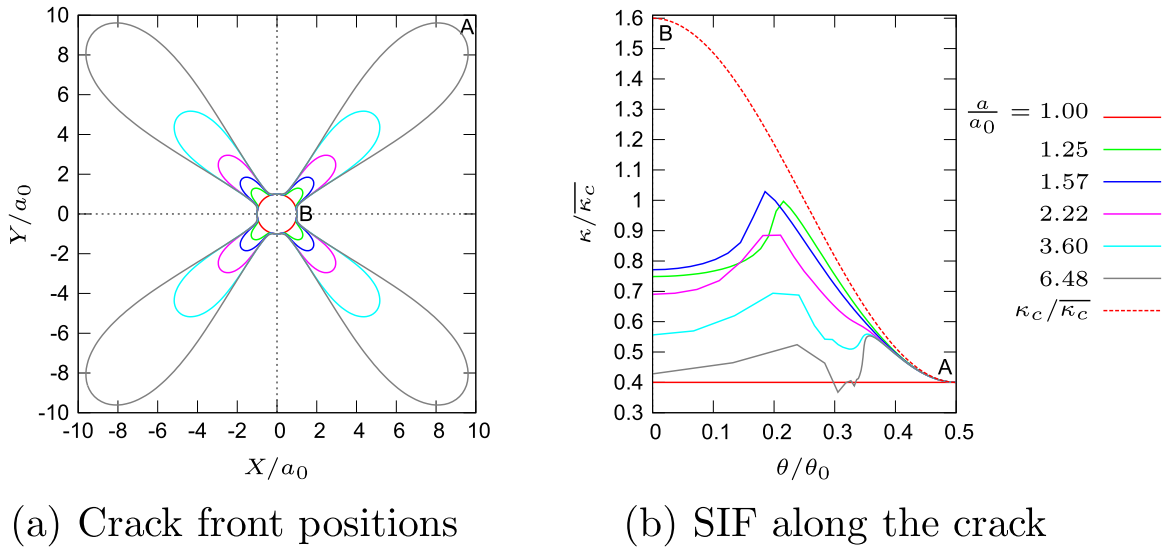

(a) Crack front positions (b) SIF along the crack

Fig. 10. Successive crack front positions and SIF along the crack front during propagation in the fingering regime for $\Delta = 0.6$ and $k=4$. (For interpretation of the references to color in this figure caption, the reader is referred to the web version of this paper.)

stationary growth. This scenario is similar to the one depicted from the first-order analysis of Section 4.1 valid in the limit $\Delta \ll 1$. The fingering regime arises from the unexpected change of behavior of the driving force in B that starts to decrease when the petal size extends beyond some critical value. For sufficiently strong obstacles, the petals reach this critical size so that the equilibrium condition is never met in B while the crack continues to grow in A.

7. Discussion

7.1. From local growth mechanism to effective fracture properties

We now come back on the relation between micro and macroscale fracture properties and provide explanation for the two distinct branches evidenced on the variations of the effective properties with the obstacle strength in Figs. 4 and 6.

We first discuss the variations of the *apparent toughness* with the obstacle strength in both regimes.

- For weak obstacles $\Delta < \Delta_c(k)$, the apparent toughness K_c is equal, within the numerical precision, to the average toughness $\overline{\kappa_c}$. As shown previously, this regime corresponds to a weak pinning of the crack that maintains an equilibrium shape satisfying $\kappa = \kappa_c$ everywhere.
  To understand why $K_c \simeq \overline{\kappa_c}$, it is fruitful to consider the evolution of the normalized SIF $\hat{\kappa}$ at the point I on the front located at $\theta = \pi/2k$ (see Fig. 1). At point I, the local toughness is equal to the average toughness $\overline{\kappa_c}$, and balances the local SIF so that $\overline{\kappa_c} = \kappa(I) = 2\sigma_c\sqrt{a/\pi}\,\tilde{\kappa}(I)$. Using Eq. (5), this gives $K_c = \overline{\kappa_c}/\tilde{\kappa}(I)$ so that K_c depends on the value of the dimensionless SIF $\tilde{\kappa}$ at point I. For small contrasts, when the first order approximation applies, the front is sinusoidal and $\tilde{\kappa}(I) = 1$ (Section 4.1). As the contrast increases and non-linear effects take place, we observe that the computed value of $\tilde{\kappa}(I)$ is still equal to one (see C.2), which means that for our flower shape cracks, the mean value of the SIF is found to be equal to the one of a circular crack of the same area. This implies $K_c = \overline{\kappa_c}$. This property, although striking, is specific to circular cracks since for the case of a semi-infinite crack perturbed by a sinusoidal toughness field, the apparent toughness is *smaller* than the average toughness (Vasoya, 2014).
- In the fingering regime, the apparent toughness is significantly smaller than the average one, and decays with the contrast. To explain this effect, we remind that the threshold is only reached around the points A so that $\frac{2}{\sqrt{\pi}}\sigma_c\sqrt{a}\tilde{\kappa}(A) = \kappa_c^{\min} = (1-\Delta)\overline{\kappa_c}$. Now, we found numerically (see Appendix C) that in the fingering regime, the SIF κ at point A is disconnected from its value at point B and corresponds approximately to the one of a circular crack of radius $R(A)$, $R(A)$ being the local radius of curvature at the end of the petals. This provides the following variations of the apparent toughness

$$\frac{K_c^a}{\overline{\kappa_c}} \sim \frac{1-\Delta}{\sqrt{R(A)/a}} \tag{23}$$

that captures qualitatively well the numerical results of Fig. 4.

We now discuss the value of the *effective fracture energy*.

- In the weak pinning regime, the front shape is known at the first order in Δ, as shown in Section 4.1. This can be used to calculate the effective fracture energy at the *second* order in Δ,

$$\frac{G_c}{\overline{\gamma_c}} = 1 - \frac{4}{k-1}\Delta^2 \tag{24}$$

as shown in Appendix D, since the second order term of the front shape cancels out. This prediction, represented in Fig. 6 for different values of k, captures well the numerical results as long as the contrast is below the critical value Δ_c. Qualitatively speaking, the inequality $G_c < \overline{\gamma_c}$ reflects that the arc length of the crack front located between the obstacles where $\gamma_c < \overline{\gamma_c}$ is longer than the one within the obstacle for which $\gamma_c > \overline{\gamma_c}$. Furthermore, the deformation of the front enhances this effect. Since the deformation amplitude $(\Delta a/a)^\infty$ increases with Δ or $1/k$ (Appendix E), G_c is a decaying function of Δ and $1/k$.
- In the fingering regime, G_c is close to the minimum value $\gamma_c^{\min}$ of the local field $\gamma_c(M)$ of fracture energy. This behavior results from the highly heterogeneous growth of the crack that propagates only between obstacles where γ_c is minimum. Interestingly, the effective fracture response in this regime is entirely governed by the *weakest* material points of the fracture plane due to the emergence of fingers. This contrasts with another regime of crack growth referred to as *strong* pinning for which the effective fracture properties are dominated by the *strongest* material points. In that regime that can take place when $\gamma_c(M)$ varies along the crack propagation direction, crack depinning from obstacles gives rise to micro-instabilities during which $\gamma > \gamma_c$. This process results in a toughening $G_c \geq \overline{\gamma_c}$ of the material and the effective fracture energy can be as large as $\gamma_c^{\max}$ (Patinet et al., 2013b; Deméry et al., 2014). The characterization of these two crack propagation regimes illustrates how the spatial arrangement of obstacles plays a central role in determining the fracture properties of heterogeneous media that can give rise to a wide range of effective behaviors within $\gamma_c^{\min} \leq G_c \leq \gamma_c^{\max}$.

We now discuss the validity of Irwin's relation at the global scale. In the weak pinning regime, we have found $K_c \simeq \overline{\kappa_c}$ and $G_c < \overline{\gamma_c}$ implying $\frac{1-\nu^2}{E}K_c^2 > G_c$. This inequality also remains true in the fingering regime where $K_c > \kappa_c^{\min}$ and $G_c \simeq \gamma_c^{\min}$. This means that the equivalence between a loading and an energy based criterion valid at the microscale thanks to Irwin's relation (3) does not survive at the macroscopic scale.

7.2. Case $k \gg 1$

An interesting limit is $k \to \infty$ that corresponds to a semi-infinite straight crack pinned by a periodic array of obstacles as it amounts to consider very small obstacles $\xi/a \to 0$ compared to the crack radius of curvature. By extrapolating the phase-diagram of Fig. 8, one observes that the fingering domain shrinks to zero since $\Delta_c \underset{k\to\infty}{\longrightarrow} 1$. This observation agrees with the variations of the effective fracture properties with k (Figs. 4 and 6) that show behaviors $K_c \underset{k\to\infty}{\longrightarrow} \overline{\kappa_c}$ and $G_c \underset{k\to\infty}{\longrightarrow} \overline{\gamma_c}$ consistent with a weak pinning of the crack without fingering.

The sole length scale remaining in this limit is the obstacle width ξ, since the medium is assumed to be infinite and the loading to be applied remotely. On the contrary, the fingering observed for circular cracks of finite size seems to appear when the obstacle size and the front deformation emerging from it are of the same order than the crack itself. Therefore, the departure of the effective properties from their mean value may occur when the obstacle size competes with another length scale like the crack length as the situation explored by Leblond et al. (1996), the distance of the loading to the crack front as in Patinet et al. (2013a) or the thickness of the body as in Ghatak et al. (2000) and Adda-Bedia and Mahadevan (2006).

8. Conclusion

When a crack propagates in a highly heterogeneous brittle interface, the front is locally slowed down or even trapped when encountering tougher material. The induced front deformation results in a selection of local toughness values that reflects at larger scale on the material resistance. The effects of this deformation on the macroscopic fracture properties were here quantified in the quasi-static limit by introducing two complementary macroscopic properties: an apparent toughness K_c defined from the loading required to make the crack propagate and an effective fracture energy G_c defined from the rate of energy released by unit area of crack advance. The relationship between these homogenized properties and the features of the local toughness map were computed using an iterative perturbation method.

Several lessons were learnt from the application of this approach to a circular crack pinned by a periodic array of defects invariant in the propagation direction.

- Irwin's relation, although valid at the microscale between κ_c and γ_c, does not survive at the macroscale between K_c and G_c, so loading and energy based approaches are no more equivalent.

- Depending on the heterogeneities size and strength, two different regimes of propagation may exist: a weak pinning regime where the propagation threshold is reached all along the front so that the whole front advances or a strong pinning regime characterized by the continuous growth of localized regions of the fronts while the other parts remain trapped.
- Correlatively, the evolution of the macroscopic fracture properties with the obstacle strength Δ may be discontinuous. While the effective properties remain close to the material average values in the weak pinning regime, they dramatically drop to the weakest value in the strong pinning regime.

This study proves the efficiency of the methodology followed to bridge the micro to the macroscale fracture properties that is applicable to various crack geometries and any toughness field. On a broader perspective, we believe that this approach can be used as a powerful tool for the rational design of heterogeneous brittle solids and interfaces with tailored failure properties.

Acknowledgements

The support of the city of Paris through the Emergence program (LP) and of the ANR Program SYSCOMM (ANR-09-SYSC-006) (VL) are gratefully acknowledged.

We also wish to thank J.-B. Leblond, K. Ravi-Chandar and D. Vandembroucq for stimulating discussions.

Appendix A. Stability of the numerical scheme

Since our numerical resolution is explicit, some numerical instabilities may occur for some values of the spatial (number of nodes N) and temporal discretization (given by $\delta a_{\max}$), as when Eulerian explicit scheme is used to solve classical partial differential equations. But physically, in the case of a homogeneous toughness field, the circular crack shape is stable towards any small perturbations of the crack shape (Gao and Rice, 1987). Also, to test the stability of our numerical scheme, we introduce artificially some small perturbation of the crack front and study under what condition on N and $\delta a_{\max}$, this small perturbation disappears during propagation. The numerical stability map obtained depends on the value of β and is given in Fig. A1. In practice, for a given value of β, the number of nodes N and the $\delta a_{\max}$ have to be chosen below those curves to ensure the stability of the numerical scheme.

Appendix B. Crack shape and SIF evolutions for $k=1$ to 6

In Section 6.3, we present all the results by discussing the $k=4$ case. For the sake of completeness, we give in this appendix, the results for other values of k. Figure B1 corresponds to the stable regime $(\Delta < \Delta_c(k))$: in each case, a stationary regime for which $\kappa = \kappa_c$ all along the front is reached. Figures B3 corresponds to the fingering one $(\Delta > \Delta_c(k))$, in which some parts of the front remain pinned forever, whereas the other parts develop in infinitely growing petals. The $k=1$ case is particular (Fig. B2), since no stable regime can then be reached if $\Delta \neq 0$.

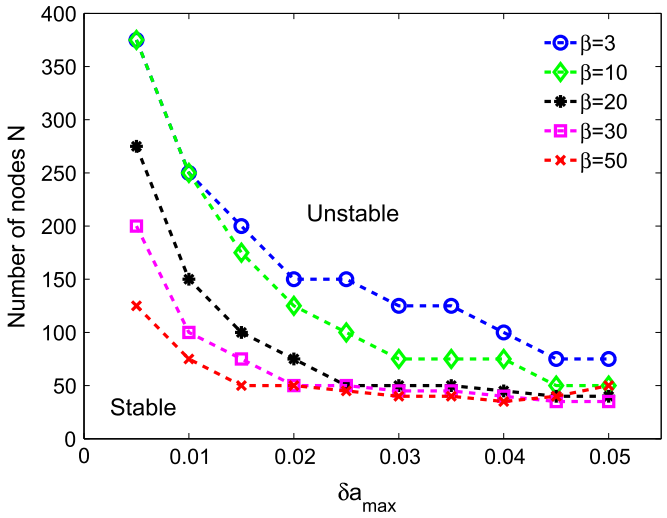

Fig. A1. Stability diagram of the numerical integration scheme.

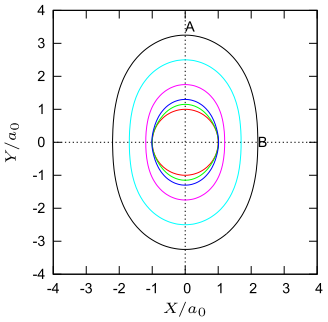

(a) $k = 2$, $\Delta = 0.1$

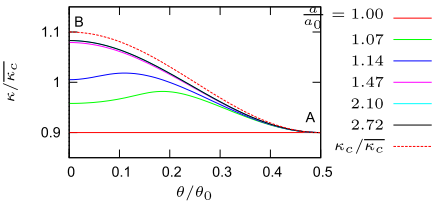

(b) $k = 2$, $\Delta = 0.1$

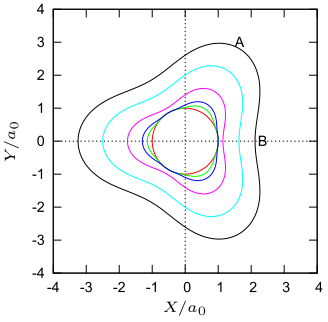

(c) $k = 3$, $\Delta = 0.2$

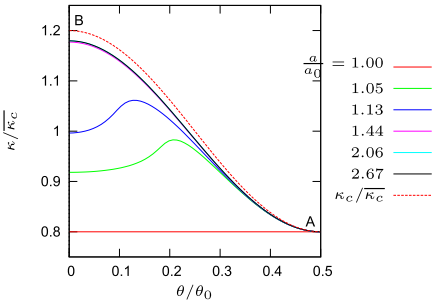

(d) $k = 3$, $\Delta = 0.2$

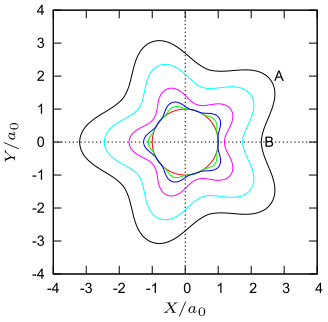

(e) $k = 5$, $\Delta = 0.3$

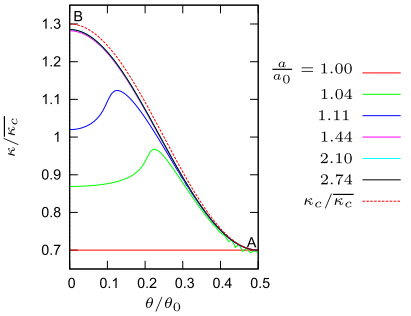

(f) $k = 5$, $\Delta = 0.3$

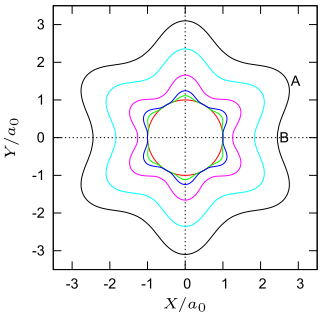

(g) $k = 6$, $\Delta = 0.3$

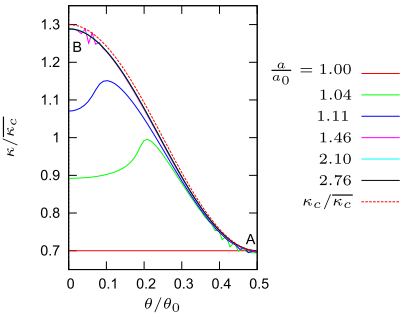

(h) $k = 6$, $\Delta = 0.3$

Fig. B1. Successive crack front positions and SIF along the crack front during propagation in the stable regime, for several values of k and Δ.

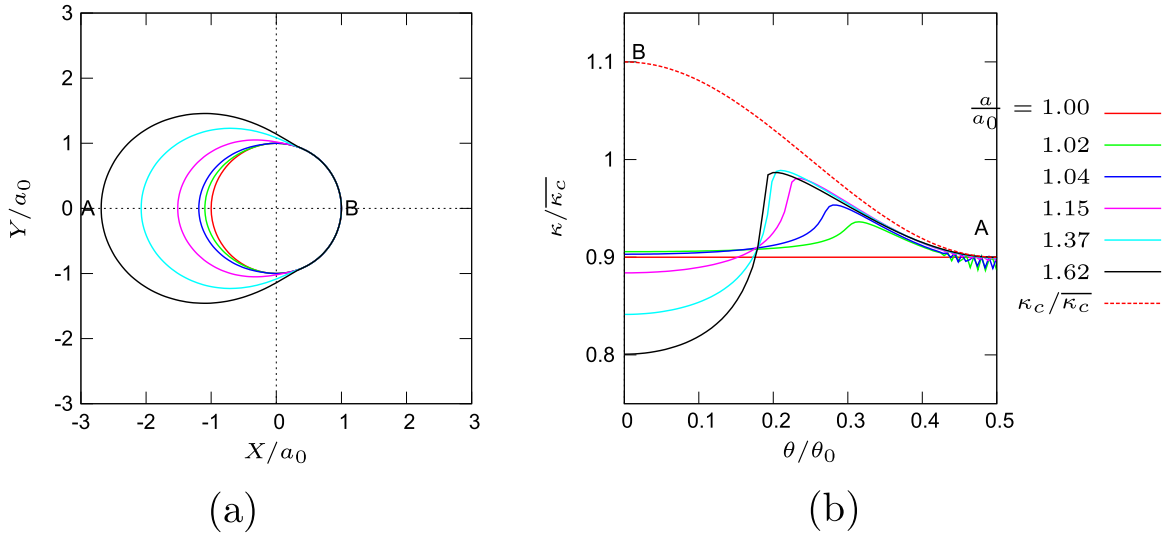

Fig. B2. Successive crack front positions and SIF along the crack front during propagation in the fingering regime for $k=1$ and $\Delta = 0.1$.

Appendix C. SIF along flower-shape crack fronts

In addition to the propagation of a crack knowing the advance law, the code provides also for each flower crack shape we encountered, the values of the SIF along the crack front. They are useful to interpret some results concerning the study of the propagation of the present paper. But they may also serve as benchmarks for other numerical SIF calculation methods. We now discuss these values in correspondence with these shapes independently from any advance law.

For this, we remove by linearity, the loading from the SIF and concentrate on the, geometry dependent, functions $\tilde{\kappa}$ and $\hat{\kappa}$ defined by:

$$\kappa(\theta) = \frac{2}{\sqrt{\pi}}\sigma\sqrt{a}\tilde{\kappa}(\theta) = \frac{2}{\sqrt{\pi}}\sigma\sqrt{a_0}\hat{\kappa}(\theta), \tag{C.1}$$

in agreement with previous notations (10) and (17). With these notations, we have $\tilde{\kappa} = 1$ for a circular crack of radius a and $\hat{\kappa} = 1$ for a circular crack of radius a_0. Both $\tilde{\kappa}$ and $\hat{\kappa}$ depend on θ and the crack shape, which themselves depend on k and Δ through the advance law. Whereas $\hat{\kappa}$ depends on the shape and size of the crack, $\tilde{\kappa}$ depends only on its shape.

In the stable regime, a stationary shape for which $\kappa = \kappa_c$ along the whole front is reached. For this shape, $\tilde{\kappa}$ has the following form:

$$\frac{\tilde{\kappa}(\theta) - \tilde{\kappa}_{\mathrm{m}}}{\Delta} = \frac{1}{2}\cos(k\theta),$$

where $\tilde{\kappa}_{\mathrm{m}}$ denotes the mean value of $\tilde{\kappa}$ along the front. The value of $\tilde{\kappa}_{\mathrm{m}}$, like $\tilde{\kappa}$, depends only on the shape of the front, and has been calculated numerically. We found surprisingly $\tilde{\kappa}_{\mathrm{m}} = 1$ for all the stationary flower shapes encountered, so that:

$$\tilde{\kappa} = 1 + \frac{\Delta}{2}\cos(k\theta) \tag{C.2}$$

In the fingering regime, the shape evolves constantly. As illustration, we consider the cases of Fig. 10 and now plot the evolution of functions $\tilde{\kappa}$ and $\hat{\kappa}$ (Fig. C1). It can be observed that after a transitory phase, $\tilde{\kappa}(A)$ and $\hat{\kappa}(B)$ become nearly invariant during the propagation (red and gray curves). This means that when the fingers become long enough, the SIF around points A and B are disconnected: around point A, its value depends on the stationary shape of the end of the petals, and around point B, it depends on the initial radius a_0. More precisely, looking at their values for different k and Δ, we found that approximate values can be provided by:

$$\kappa(A) \simeq \alpha_A \frac{2}{\sqrt{\pi}}\sigma\sqrt{R(A)} \tag{C.3}$$

$$\kappa(B) \simeq \alpha_B \frac{2}{\sqrt{\pi}}\sigma\sqrt{a_0} \tag{C.4}$$

where $R(A)$ is the local radius of curvature at point A, $\alpha_A \in [1;\ 1.2]$ and $\alpha_B \in [1;\ 2]$ for the different values of $k \leq 8$ and $\Delta \leq 0.9$ tested here.

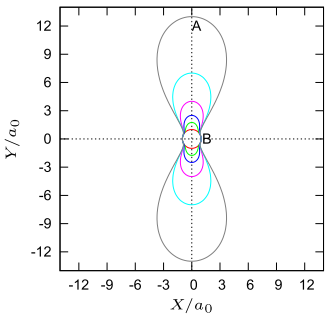

(a) $k = 2$, $\Delta = 0.4$

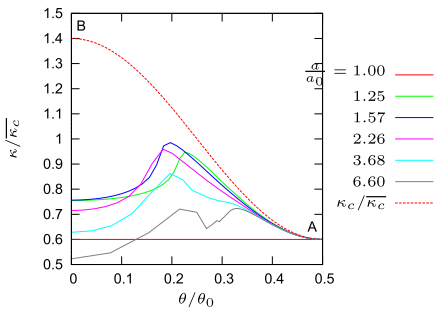

(b) $k = 2$, $\Delta = 0.4$

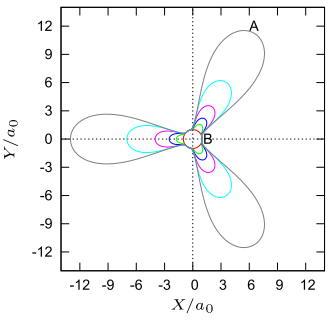

(c) $k = 3$, $\Delta = 0.5$

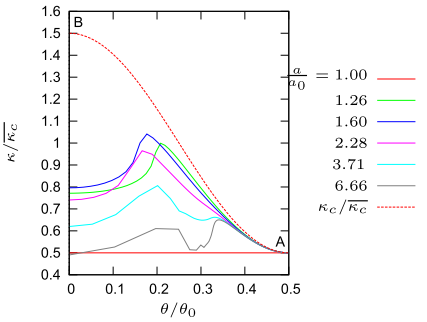

(d) $k = 3$, $\Delta = 0.5$

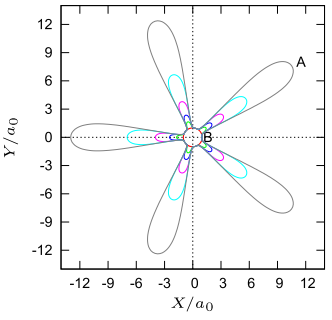

(e) $k = 5$, $\Delta = 0.7$

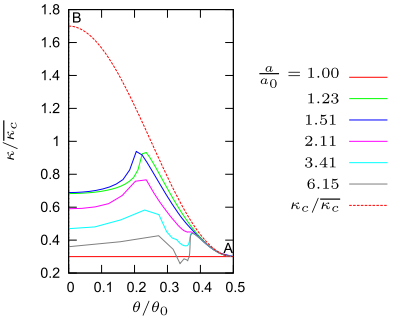

(f) $k = 5$, $\Delta = 0.7$

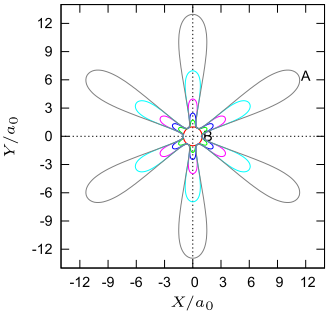

(g) $k = 6$, $\Delta = 0.6$

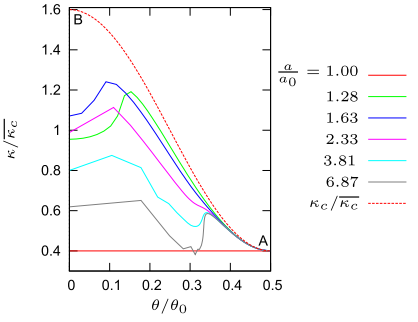

(h) $k = 6$, $\Delta = 0.6$

Fig. B3. Successive crack front positions and SIF along the crack front during propagation in the fingering regime, for several values of k and Δ.

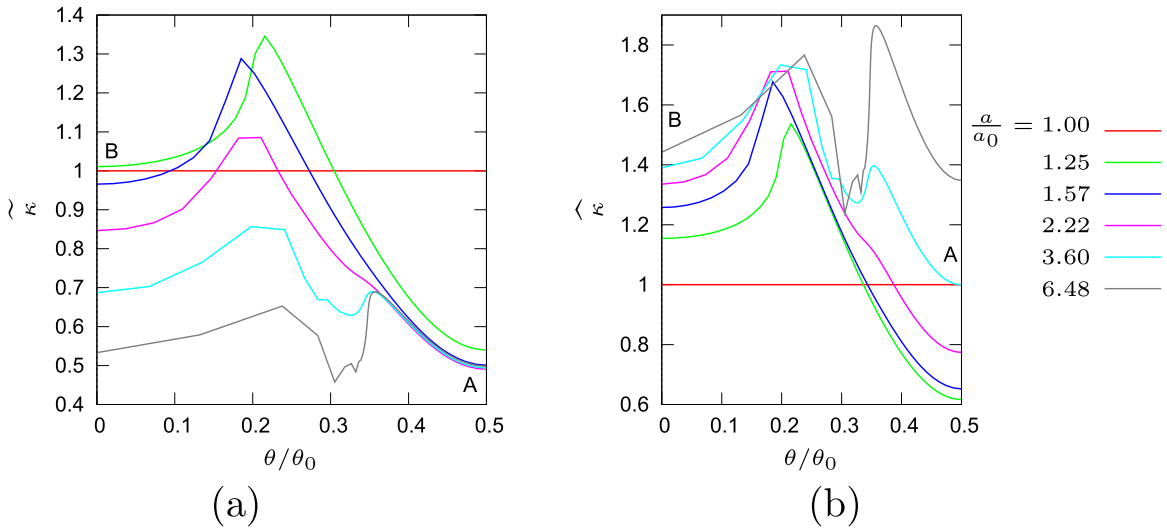

Fig. C1. Distribution of dimensionless SIF (a) $\tilde{\kappa}$ and (b) $\hat{\kappa}$ along the crack front corresponding to different successive equilibrium positions of Fig. 10 ($k = 4$, $\Delta = 0.6$).

Appendix D. Asymptotic expansion of $\frac{G_c}{\overline{\gamma_c}}$ to the second order in Δ

To each value of k and Δ in the weak pinning regime corresponds an equilibrium crack shape characterized by its polar equation that we denote $a_{\mathrm{eq}}(\theta)$. Elementary geometric considerations about polar curves gives

$$\frac{G_c}{\overline{\gamma_c}} = \frac{\int_{-\pi}^{\pi} \frac{\gamma_c(\theta)}{\overline{\gamma_c}} a_{\mathrm{eq}}^2(\theta)\mathrm{d}\theta}{\int_{-\pi}^{\pi} a_{\mathrm{eq}}^2(\theta)\mathrm{d}\theta} \tag{D.1}$$

where the equilibrium condition $\gamma = \gamma_c$ all along the front and the definition (6) of G have been used.

Now, thanks to (21), we know that for $\Delta \ll 1$, $a_{\mathrm{eq}}(\theta)/a = 1 - \frac{2\Delta}{k-1}\cos(k\theta) + \Delta^2 a_2(\theta) + O(\Delta^3)$, where we denote $a_2(\theta)$ the second order term. Using this expression and Eq. (19)) for γ_c, we find that a_2 cancels out in the asymptotic expansion of (D.1), so that finally:

$$\frac{G_c}{\overline{\gamma_c}} = 1 - \frac{4}{k-1}\Delta^2 + O(\Delta^3). \tag{D.2}$$

Appendix E. Stationary amplitude of front deformation in the weak pinning regime

Fig. E1 shows the asymptotic value of the normalized petal amplitude $(\Delta a/a)^{\infty} = \lim_{a\to\infty} \frac{\Delta a(a)}{a}$ measured during the stationary part of the crack growth (see Fig. 7). $(\Delta a/a)^{\infty}$ is defined in the weak pinning regime only, so for $\Delta < \Delta_c(k)$, and corresponds to the petal size of the front at equilibrium. These numerical predictions are verified to be in agreement with the first order theory of Eq. (21). It can be noticed that this amplitude increases, without surprise, with the obstacle strength Δ. Less obvious is its increase with $1/k$, that is with the heterogeneity size, which basically results from the fact that the crack front has more space to develop.

References

Adda-Bedia, M., Mahadevan, L., 2006. Crack-front instability in a confined elastic film. Proc. R. Soc. A Math. Phys. Eng. Sci. 462 (2075), 3233–3251.
Barthelat, F., Tang, H., Zavattieri, P.D., Li, C.M., Espinosa, H.D., 2007. On the mechanics of mother-of-pearl: a key feature in the material hierarchical structure. J. Mech. Phys. Solids 55, 306–337.
Barthelat, F., Rabiei, R., 2011. Toughness amplification in natural composites. J. Mech. Phys. Solids 59, 829–840.
Bower, A.F., Ortiz, M., 1990. Solution of three-dimensional crack problems by a finite perturbation method. J. Mech. Phys. Solids 38 (4), 443–480.
Bower, A.F., Ortiz, M., 1991. A three-dimensional analysis of crack trapping and bridging by tough particles. J. Mech. Phys. Solids 39 (6), 815–858.
Bueckner, H.F., 1987. Weight functions and fundamental fields for the penny-shaped and the half-plane crack in three-space. Int. J. Solids Struct. 23 (1), 57–93.
Dalmas, D., Barthel, E., Vandembroucq, D., 2009. Crack front pinning by design in planar heterogeneous interfaces. J. Mech. Phys. Solids 57 (3), 446–457.
Demery, V., Rosso, A., Ponson, L., 2014. From microstructural features to effective toughness in disordered brittle solids. EPL 105, 34003.
Dimas, L.S., Giessa, T., Buehler, M.J., 2014. Coupled continuum and sicrete analysis of random heterogeneous materials: elasticity and fracture. J. Mech. Phys. Solids 63, 481–490.

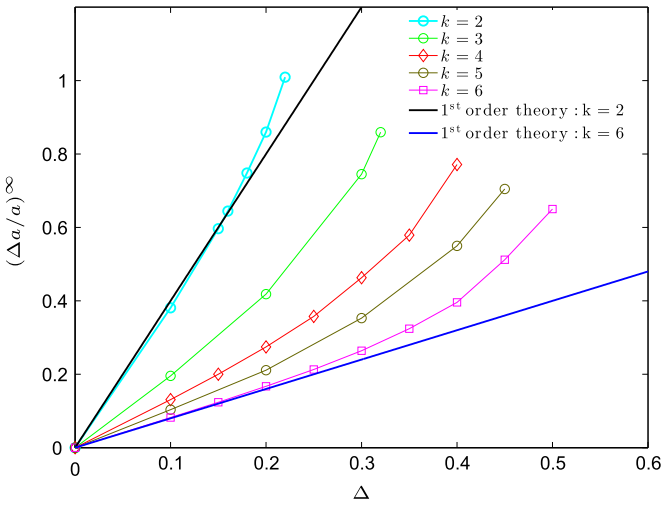

Fig. E1. Influence of k and Δ on the normalized petal size $(\Delta a/a)^{\infty}$ in the asymptotic stable regime.

Favier, E., Lazarus, V., Leblond, J.-B., 2006. Coplanar propagation paths of 3D cracks in infinite bodies loaded in shear. Int. J. Solids Struct. 43 (7–8), 2091–2109.

Gao, H., 1988. Nearly circular shear mode cracks. Int. J. Solids Struct. 24 (2), 177–193.

Gao, H., 1991. Fracture analysis of nonhomogeneous materials via a moduli-perturbation approach. Int. J. Solids Struct. 27 (13), 1663–1682.

Gao, H., Rice, J.R., 1987. Somewhat circular tensile cracks. Int. J. Fract. 33 (3), 155–174.

Gao, H., Rice, J.R., 1989. A first-order perturbation analysis of crack trapping by arrays of obstacles. Trans. ASME 56, 828–836.

Ghatak, A., Chaudhury, M.K., Shenoy, V., Sharma, A., 2000. Meniscus instability in a thin elastic film. Phys. Rev. Lett. 85, 4329–4332.

Hossain, M.Z., Hsueh, C.J., Bourdin, B., Bhattacharya, K., 2014. Effective toughness of heterogeneous media. J. Mech. Phys. Solids 71 (November), 15–32.

Irwin, G.R., 1957. Analysis of stresses and strains near the end of a crack traversing a plate. J. Appl. Mech. 24, 361–364.

Kachanov, M., 1994. Elastic solids with many cracks and related problems. In: Hutchinson, J., Wu, T. (Eds.), Advances in Applied Mechanics, Academic Press, London, pp. 259–445.

Lai, Y.-S., Movchan, A.B., Rodin, G.J., 2002. A study of quasi-circular cracks. Int. J. Fract. 113, 1–25.

Lazarus, V., 2003. Brittle fracture and fatigue propagation paths of 3D plane cracks under uniform remote tensile loading. Int. J. Fract. 122 (1–2), 23–46.

Lazarus, V., 2011. Perturbation approaches of a planar crack in linear elastic fracture mechanics: a review. J. Mech. Phys. Solids 59 (2), 121–144.

Lazarus, V., Leblond, J.-B., 2002. In-plane perturbation of the tunnel-crack under shear loading. II: determination of the fundamental kernel. Int. J. Solids Struct. 39 (17), 4437–4455.

Leblond, J.-B., Mouchrif, S.-E., Perrin, G., 1996. The tensile tunnel-crack with a slightly wavy front. Int. J. Solids Struct. 33 (14), 1995–2022.

Leblond, J.-B., Patinet, S., Frelat, J., Lazarus, V., 2012. Second-order coplanar perturbation of a semi-infinite crack in an infinite body. Eng. Fract. Mech. 90 (0), 129–142.

Legrand, L., Patinet, S., Leblond, J.B., Frelat, J., Lazarus, V., Vandembroucq, D., 2011. Coplanar perturbation of a crack lying on the mid-plane of a plate. Int. J. Fract. 170, 67–82.

Patinet, S., Alzate, L., Barthel, E., Dalmas, D., Vandembroucq, D., Lazarus, V., 2013a. Finite size effects on crack front pinning at heterogeneous planar interfaces: experimental, finite elements and perturbation approaches. J. Mech. Phys. Solids 61 (2), 311–324.

Patinet, S., Frelat, J., Lazarus, V., Vandembroucq, D., 2011. Propagation des fronts de fissure plane dans les matériaux fragiles hétérogènes de dimensions finies. Méc. Ind. 12 (3), 199–204.

Patinet, S., Vandembroucq, D., Roux, S., 2013b. Quantitative prediction of effective toughness at random heterogeneous interfaces. Phys. Rev. Lett. 110, 165507.

Pindra, N., Lazarus, V., Leblond, J.-B., 2010. In-plane perturbation of a system of two coplanar slit-cracks—I: case of arbitrarily spaced crack fronts. Int. J. Solids Struct. 47, 3489–3503.

Rice, J.R., 1985. First-order variation in elastic fields due to variation in location of a planar crack front. ASME J. Appl. Mech. 52 (3), 571–579.

Rice, J.R., 1989. Weight function theory for three-dimensional elastic crack analysis. In: Wei, R. P., Gangloff, R. P. (Eds.), Fracture Mechanics: Perspectives and Directions (Twentieth Symposium). American Society for Testing and Materials, STP 1020, Philadelphia, USA, pp. 29–57.

Ritchie, R.O., 2011. The conflicts between strength and toughness. Nat. Mater. 10 (November (11)), 817–822.

Roux, S., Vandembroucq, D., Hild, F., 2003. Effective toughness of heterogeneous brittle materials. Eur. J. Mech. A/Solids 22 (5), 743–749.

Saffman, P.G., Taylor, G.I., 1958. The penetration of a fluid into a porous medium of hele-shaw cell containing a more viscous liquid. Proc. R. Soc. London A 245, 312.

Saintyves, B., Dauchot, O., Bouchaud, E., 2013. Bulk elastic fingering instability in hele-shaw cells. Phys. Rev. Lett. 111, 047801.

Vasoya, M., November 2014. Study on Tensile Failure of Highly Heterogeneous Materials. (Ph.D. thesis), Université Pierre et Marie Curie - Paris VI, Paris. ⟨https://hal.archives-ouvertes.fr/tel-01091968⟩.

Vasoya, M., Leblond, J.-B., Ponson, L., 2013. A geometrically nonlinear analysis of coplanar crack propagation in some heterogeneous medium. Int. J. Solids Struct. 50 (2), 371–378.

Vasoya, M., Unni, A.B., Leblond, J.-B., Lazarus, V., Ponson, L., 2016. Finite size and geometrical non-linear effects during crack pinning by heterogeneities: an analytical and experimental study. J. Mech. Phys. Solids. 89, 211–230.

Weibull, A., 1939. Statistical theory of the strength of materials. Proc. R.-Swed. Inst. Eng. Res. 151, 145.

Willis, J.R., 2013. Crack front perturbations revisited. Int. J. Fract. 184 (November (1–2)), 17–24.

Xia, S., Ponson, L., Ravichandran, G., Bhattacharya, K., 2015. Adhesion of heterogeneous thin films: II. Adhesive heterogeneity. J. Mech. Phys. Solids 83, 88–103.